

Imaging with flat optics: metalenses or diffractive lenses?

Sourangsu Banerji,¹ Monjurul Meem,¹ Berardi Sensale-Rodriguez¹ and Rajesh Menon^{1,2,a)}

¹Department of Electrical and Computer Engineering, University of Utah, Salt Lake City, UT 84112, USA.

²Oblate Optics, Inc. 13060 Brixton Place, San Diego CA 92130, USA.

a) rmenon@eng.utah.edu

ABSTRACT

Recently, there has been an explosion of interest in metalenses for imaging. The interest is primarily based on their sub-wavelength thicknesses. Diffractive lenses have been used as thin lenses since the late 19th century. Here, we show that multi-level diffractive lenses (MDLs), when designed properly can exceed the performance of metalenses. Furthermore, MDLs can be designed and fabricated with larger constituent features, making them accessible to low-cost, large area volume manufacturing, which is generally challenging for metalenses. The support substrate will dominate overall thickness for all flat optics. Therefore the advantage of a slight decrease in thickness (from $\sim 2\lambda$ to $\sim \lambda/2$) afforded by metalenses may not be useful. We further elaborate on the differences between these approaches and clarify that metalenses have unique advantages when manipulating the polarization states of light.

INTRODUCTION

Lenses are fundamental to imaging systems. Conventional lenses exploit refraction to focus light [1]. As a result, a fundamental trade-off increases the thickness and weight of optics with increasing numerical aperture (or resolution). As illustrated in Fig. 1a with the example of a simple plano-convex lens, larger bending angles require larger thicknesses. Recently, there has been significant interest in reducing the thickness and weight of lenses by exploiting diffraction. In such “flat-lenses,” focusing is achieved by spatially arranging “zones” that impart appropriate phase to achieve constructive interference of the transmitted waves at the focus [2, 3]. As illustrated in Fig. 1b, larger bending angles may be achieved with no change in thickness, simply by decreasing the local period of the diffractive structure. In order to ensure constructive interference, each ray must be locally phase shifted to compensate for the variation in its total optical path length to the focus. In traditional diffractive lenses, this is achieved by engineering the path traversed by the ray within the diffractive lens itself, as illustrated in Fig. 1c. In comparison to travelling the same distance in air, the optical path delay for a thickness, t is $\Delta = (n - 1) t$, which then corresponds to a phase shift of $\Delta/\lambda * 2\pi$, where n is the refractive index of the material and λ is the wavelength of light. In order to achieve a phase shift of 2π , t must be at least $\lambda/(n-1) \sim 2\lambda$ for $n=1.5$. It is noted that diffractive lenses with numerical aperture (NA) > 1 under water immersion were demonstrated more than a decade ago [4]. In order to increase the focusing efficiency, blazed or multi-level diffractive lenses (MDLs) were also developed to approximate the optimal continuous phase distribution (see Fig. 1d). In fact, it was widely recognized that close to 100% efficiency could be achieved with such blazed diffractive optics [5]. However, at high numerical apertures, there is a rapid drop in efficiency due to the resonance conditions [6, 7]. It was also quite definitively shown that this drop could be avoided by

parametric optimization of the geometry of the constituent structures of the diffractive lens using both simulations [7, 8] and experiments [9, 10]. Another Achilles heel for diffractive lenses has been their poor broadband performance, which was overcome for discrete wavelengths via harmonic phase shifts [11] and by using higher-orders of diffraction [12]. We extended this work to continuous broadband spectra using efficient numerical techniques [13-15] and advanced multi-level nanofabrication at visible [16-20] and Terahertz spectra [21]. *Here, we combine this multi-level approach with parametric optimization to show that high efficiency at high numerical aperture is feasible for both narrowband and broadband operation, which we believe has not been clearly demonstrated before.*

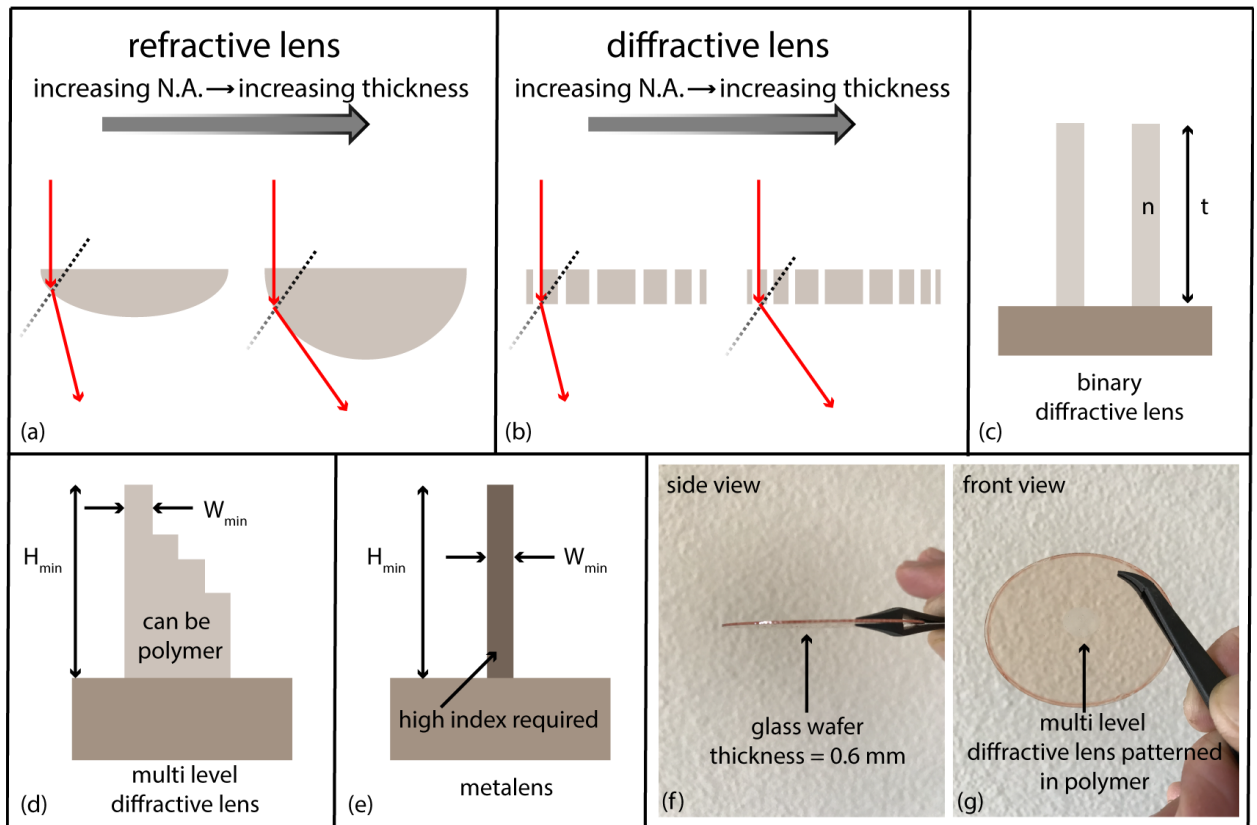


Figure 1: Bending of light via (a) refraction and (b) diffraction. Schematic of the constituent element of a (c) conventional binary diffractive lens, (d) multi-level diffractive lens (MDL) and (e) metalens. Photographs of a broadband visible MDL fabricated in a polymer film on a glass

substrate are shown in (f) side-view emphasizing the small thickness, which is dominated by the substrate and (g) front view.

Recently, metalenses were proposed as a means to reduce the overall thickness of the conventional diffractive lens to sub-wavelength regimes by exploiting magnified phase changes that can occur in resonators [22-29]. Rather than using traversed path to create a phase shift, appropriately designed subwavelength antenna elements could achieve the same effect (see Fig. 1e). In this report, we show that the advantages of metalenses might be vastly over-stated and that the decrease in thickness from about 2λ (achievable via MDLs) to less than λ may not be useful for the majority of applications. To emphasize this point, we show a photograph from the side-view (Fig. 1f) of a multi-level diffractive lens that is corrected for the visible spectrum. This device was fabricated in a polymer film atop a glass wafer (thickness~0.6mm) as shown in Fig. 1g [19,20]. We point out that the support substrate will dominate the overall thickness in all cases, and thereby obviate any advantage due to reduction in the device thickness.

We further make the case that MDLs can achieve the same or better optical performance when compared to metalenses. To illustrate this point, we first performed an exhaustive literature survey of metalenses that have been reported so far. A summary of this survey is included in the *Supplementary Information*. Then, we selected exemplary metalenses that operate in the narrowband and in the broadband spectral regimes at low, medium and high numerical apertures, and we designed MDLs having the same optical specifications (focal length, numerical aperture and operating wavelengths). Finally, we compared the focusing efficiencies of the MDLs to those of the corresponding metalenses. Table 1 summarizes the key results. The first 3 columns are the optical specifications. Comparing the focusing efficiencies in columns 6 and 9 confirm that MDLs indeed perform better than metalenses. For the MDLs, we used a commonly available

polymer photoresist (Shipley S1813) as the constituent material, since it exhibits high transmission in most wavelength regimes of interest here (measured dispersion is included in the *Supplementary Information*), and we have previously fabricated several MDLs in this material [16-20]. In all cases, we assume unpolarized input light for the MDLs.

Table 1: Summary of performance of MDL and Metalens for same optical specifications. Note that W_{\min} and H_{\max} are defined in Figs. 1d and 1e for MDL and metalens, respectively.

Narrowband			Multi-level diffractive lens			Metalens		
NA	focal length	λ	W_{\min}	H_{\max}	Efficiency	W_{\min}	H_{\max}	Efficiency
0.2	67 μm	530nm	1 μm	1.1 μm	93%	0.05 μm	0.6 μm	92% [25]
0.6	200 μm	532nm	0.4 μm	1.1 μm	90%	0.25 μm	0.6 μm	87% [26]
0.97	25 μm	1550nm	0.75 μm	3.1 μm	87%	0.2 μm	0.95 μm	72% [23]
Broadband			Multi-level diffractive lens			Metalens		
NA	focal length	λ	W_{\min}	H_{\max}	Efficiency	W_{\min}	H_{\max}	Efficiency
0.2	63 μm	470nm to 670nm	1 μm	2 μm	81%	0.08 μm	0.6 μm	50% [27]
0.35	155 μm	3 μm to 5 μm	4 μm	10 μm	86%	0.4 μm	2 μm	70% [28]
0.81	2 μm	560nm to 800nm	0.35 μm	1.6 μm	70%	0.055 μm	0.488 μm	69% [29]

Thirdly, we point out that the fabrication complexity of metalenses is far higher than those of MDLs. As can be seen in Table 1 (columns 4 and 7), the minimum feature widths required for metalenses are significantly smaller than those for MDLs. In addition, metalenses generally require high-index materials (see Tables S1 and S2 in the *Supplementary Information*), whereas MDLs can be fabricated in low-index polymers. It is important to appreciate that any

transparent material can be used for the MDL. This allows MDLs to be mass manufactured at low cost via high-volume imprinting techniques [30].

RESULTS AND DISCUSSION

Our design methodology involves nonlinear optimization to select the heights of the constituent elements of the MDL in order to maximize focusing efficiency averaged over all wavelengths of interest as described previously [18-20]. In congruence with work in metalenses, we define focusing efficiency as the ratio of the power within a spot of diameter equal to 3 times the simulated full-width at half-maximum (FWHM) to the total incident power [23]. The point-spread function of each MDL was simulated using the finite-difference time-domain method with the incident electric field polarized in the plane of the MDL. Averaging the fields over the two orthogonal polarization directions of the electric field simulates the PSF from unpolarized light. All analysis in the main text utilized this PSF assuming unpolarized input. Details of our simulation are described in the *Supplementary Information*. We note that not all papers follow a consistent method for calculating focusing efficiency. Therefore, we have included a brief description of the methods in the selected metalens papers in the *Supplementary Information*.

(1) Narrowband MDLs

First, we consider the design of MDLs for discrete wavelengths (narrowband). Following the parameters from Table 1, we designed 3 MDLs with (focal length, numerical aperture) = (67 μm , 0.2), (200 μm , 0.6) and (25 μm , 0.97).

The optimized designs represented by the height distribution of the concentric rings are illustrated in Figs. 2a, 2c and 2e for NA=0.2, 0.6 and 0.97 MDLs, respectively. The corresponding simulated point-spread functions (PSFs) are shown in Figs. 2b, 2d and 2f,

respectively. The FWHM noted in the insets of the PSFs confirm close to diffraction-limited performance. The simulations confirm that even at NA as high as 0.97 efficiencies over 87% are maintained, which are superior to those of corresponding metalenses (Table 1). We note that shadowing effects can clearly impact focusing efficiencies at high NA for both metalenses and MDLs. Our simulations simply point out that metalenses do not offer any advantage over MDLs for narrowband operation, while exhibiting equivalent optical performance.

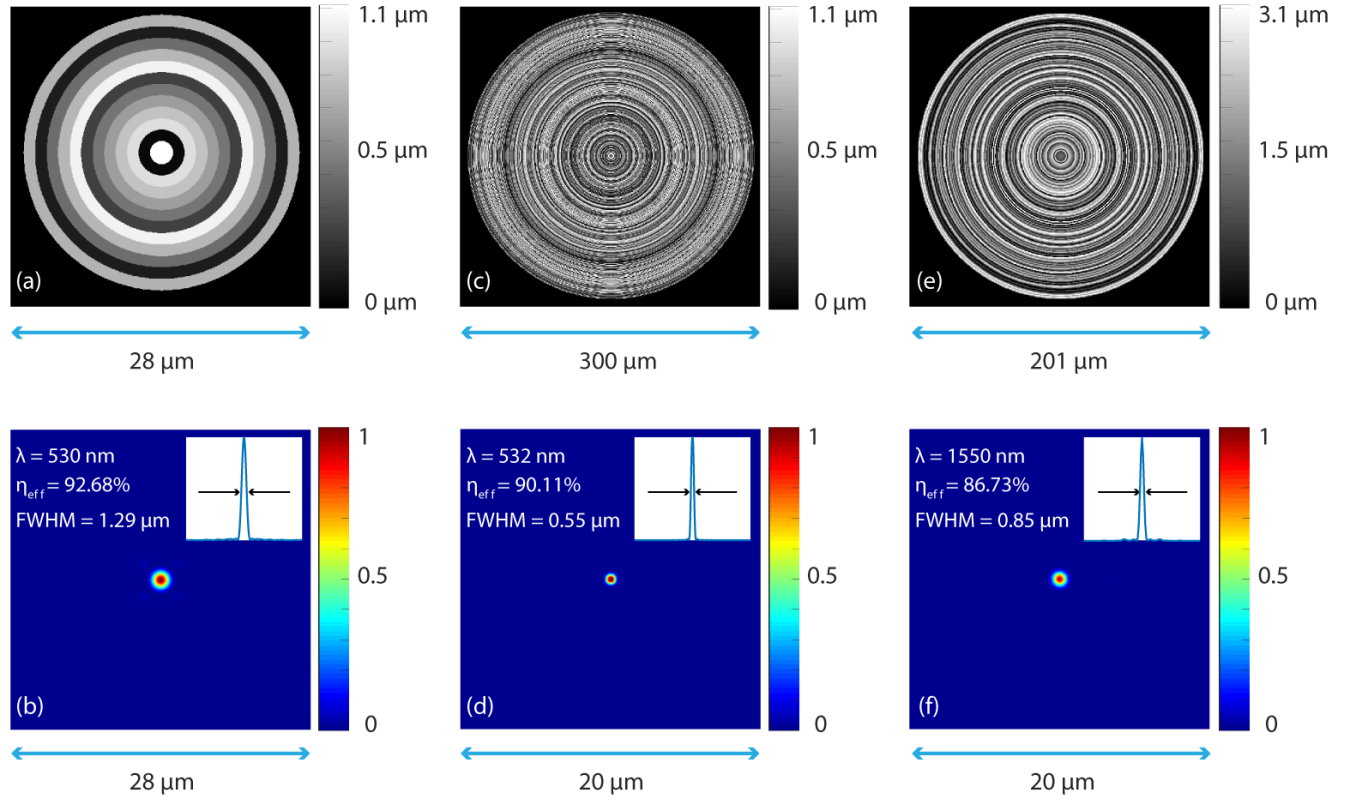


Figure 2: Narrowband MDLs. Design (top row) and simulated point-spread function (bottom row) for low (a, b), medium (c, d) and high-NA (e, f) MDLs are shown.

(2) Broadband MDLs

One of the big advantages of MDLs as we have pointed out before is their good achromatic performance over broad spectral bands [18-21]. Here, we reiterate this claim by directly comparing MDLs with metalenses of the same optical specifications. Again, following the parameters from Table 1, we designed 3 broadband MDLs with (focal length, numerical

aperture) = (63 μ m, 0.2), (200 μ m, 0.36) and (2 μ m, 0.81). The optimized designs represented by the height distribution of the concentric rings are illustrated in Figs. 3a, 3f and 3k for NA=0.2, 0.36 and 0.81 MDLs, respectively. The corresponding simulated point-spread functions (PSFs) for 3 representative wavelengths are shown in Figs. 3b-d, 3g-i and 3l-n, respectively. Again, the FWHM noted in the insets of the PSFs confirm close to diffraction-limited performance for all wavelengths. The simulations confirm that even at NA as high as 0.81 efficiencies of 70% are maintained across the entire band, which are superior to those of corresponding metalenses (Table 1).

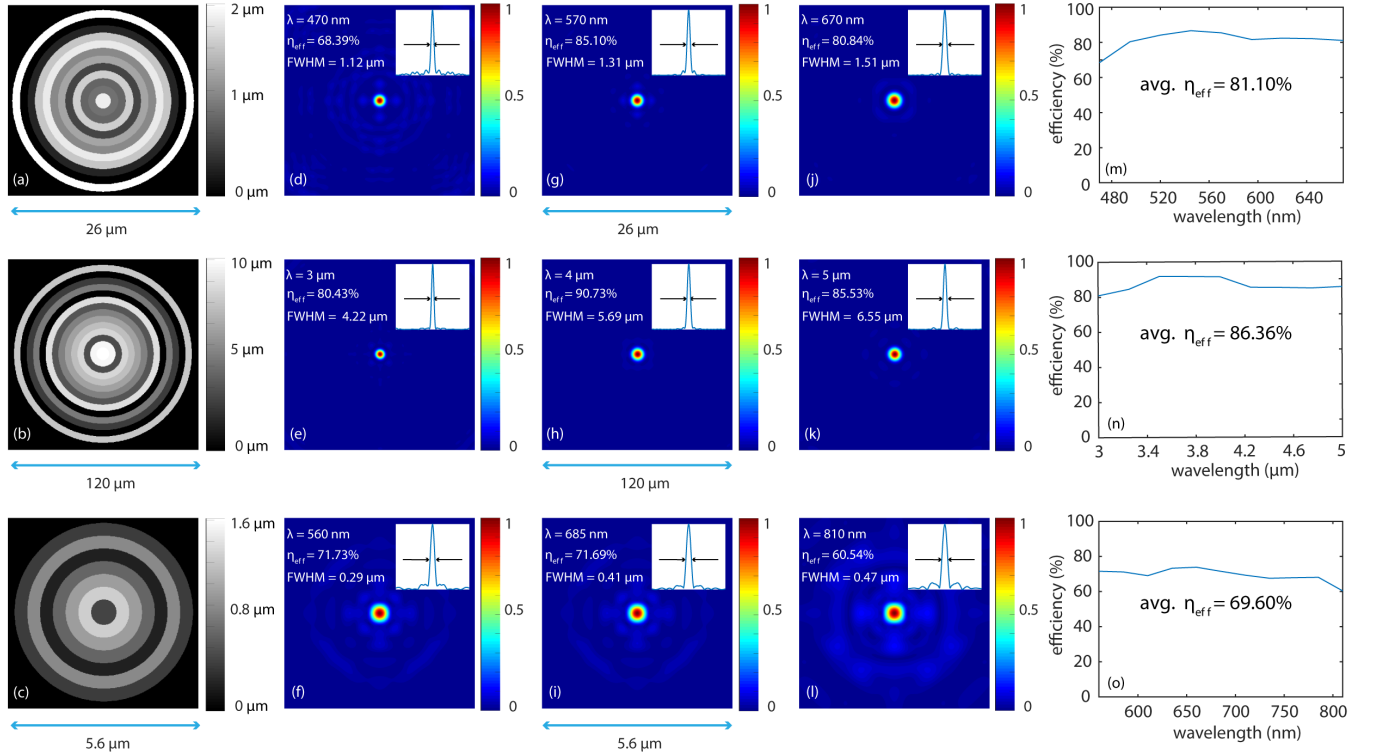


Figure 3: Broadband MDLs. Design (a-c) and simulated point-spread functions (d-l) and simulated focusing efficiency spectra (m-o) for low, medium and high-NA MDLs.

(3) Aberrations analysis

When illuminated by a normally incident uniform plane wave, an ideal lens will generate a perfectly spherical wavefront that converges to the ideal focus. Aberrations in an actual lens are

defined as the difference between the actual wavefront from this ideal wavefront. Here, we use the simulated wavefront to analyze the aberrations that are present in MDLs. Using the Zernike-polynomials representation of aberrations, we can calculate the wavefront errors as illustrated in Fig. 4 for the broadband MDL with NA=0.81, $f=2\mu\text{m}$ computed at $\lambda=560\text{nm}$. Similar results for the other lenses as well as details of the aberrations analysis are included in the *Supplementary Information*.

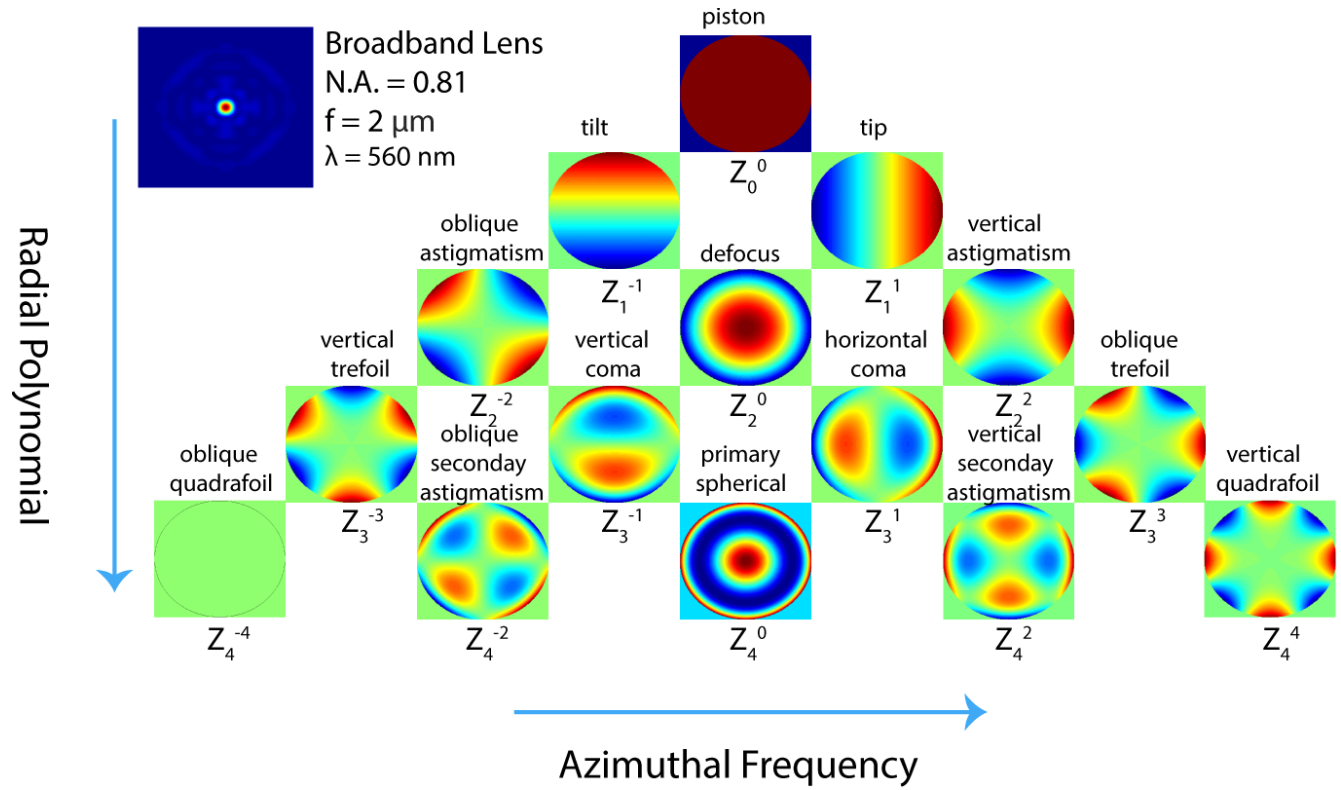


Figure 4: Aberrations-analysis in form of Zernike polynomials for NA=0.81, $f=2\mu\text{m}$ MDL simulated at $\lambda=560\text{nm}$.

Furthermore, table 2 summarizes the Zernike coefficients (in units of wavelengths) for the narrowband MDL with NA=0.97, $f=25\mu\text{m}$, $\lambda=1550\text{nm}$ and the broadband MDL with NA=0.81, $f=2\mu\text{m}$ and simulated at representative wavelengths of $\lambda=560\text{nm}$, 685nm and 810nm .

These calculations confirm that MDLs have extremely low aberrations and the broadband MDLs exhibit very low variation in aberrations across the operating wavelength range.

Table 2: Zernike coefficients (in units of λ) for two exemplary high-NA MDLs; one narrowband and another broadband.

Narrowband (N.A. = 0.97)	Multi-level diffractive lens									
Wavelength	Piston	Tip	Tilt	Defocus	Vertical astigmatism	Horizontal astigmatism	Vertical coma	Horizontal coma	Oblique trefoil	Vertical trefoil
1550 nm	3.53E-05	-6.89E-22	-1.77E-22	-8.78E-05	5.78E-21	1.56E-22	7.21E-22	6.07E-22	1.36E-4	4.66E-22
Broadband (N.A. = 0.81)	Multi-level diffractive lens									
Wavelength	Piston	Tip	Tilt	Defocus	Vertical astigmatism	Horizontal astigmatism	Vertical coma	Horizontal coma	Oblique trefoil	Vertical trefoil
560 nm	1.85E-02	1.84E-19	-6.75E-20	-2.47E-2	3.10E-19	8.26E-20	2.04E-19	-9.55E-20	4.06E-2	1.65E-18
685 nm	2.16E-02	-5.61E-19	-2.08E-20	-3.26E-2	2.97E-18	7.66E-20	7.65E-19	-1.18E-19	3.18E-2	1.38E-18
810 nm	4.23E-02	-4.21E-19	4.96E-20	-4.56E-2	-2.68E-18	6.08E-20	1.90E-18	2.11E-19	2.21E-2	3.57E-18

(4) Where are meta-optics useful?

Finally, we would like to clarify the regimes where meta-optics (where we include metamaterials, metasurfaces and metalenses) have distinct advantages over MDLs and conventional diffractive optics. Meta-optics have the advantage of extreme form birefringence, which enable them to manipulate the polarization states of light in unique manners. A few illustrative examples of these advantages are in polarimetric imaging [31], high-efficiency polarizers [32] and polarization sensitive optics [33]. Additionally, their sub-wavelength dimensions are extremely useful in integrated optics and photonics, where integration density is a critical parameter for technology adoption [34-36].

CONCLUSION

Using a series of rigorous simulations, we conclude that multi-level diffractive lenses, when designed appropriately, can provide better optical performance, while being significantly

simpler to manufacture, when compared to metalenses. MDLs can exploit the relatively mature mass manufacturing capabilities that exist in the holograms industry to create low-cost large-area flat optics, enabling a new era of ultra-lightweight, thin optical systems.

Methods

All MDL designs were obtained using nonlinear optimization using a modified gradient-descent-based search algorithm that maximized wavelength-averaged focusing efficiency. The PSF simulations were performed using commercially available FDTD software from Lumerical.

References

1. Born, M. and Wolf, E. *Principle of Optics*, 7th ed. (Cambridge University Press, Cambridge, 1999).
2. Gil, D., Menon R. and Smith, H. I. The Case for Diffractive Optics in Maskless Lithography. *J. Vac. Sci. Technol. B*, **21**(6), 2810-2814, (2003).
3. Buralli, D. A. and Morris, G. M. Design of diffractive singlets for monochromatic imaging. *Appl. Opt.* **30**(16), 2151-2158 (1991).
4. Chao, D., Patel, A. A., Barwicz, T., Smith, H. I. and Menon, R. Immersion Zone-Plate-Array Lithography. *J. Vac. Sci. Technol. B*, **23**(6), 2657-2661 (2005).
5. Fleming, M. B. and Hutley, M. C. Blazed diffractive optics. *Appl. Opt.* **36**(20) 4635 (1997).
6. Petit, R. ed., *Electromagnetic Theory of Gratings* (Springer, Berlin, 1980).
7. Noponen, E., Turunen, J. and Vasara, A. Parametric optimization of multilevel diffractive optical elements by electromagnetic theory. *Appl. Opt.* **31**, 5010–5012 (1992).
8. Noponen, E., Turunen, J. and Vasara, A. Electromagnetic theory and design of diffractive-lens arrays. *J. Opt. Soc. Am. A* **10**, 434–443 (1993).
9. Finlan, J. M., Flood, K. M. and Bojko, R. J. Efficient $f:1$ binary-optics microlenses in fused silica designed using vector diffraction theory. *Opt. Eng.* **34**, 3560–3564 (1995).
10. Shiono, T., Hamamoto, T. and Takahara, K. High-efficiency blazed-diffractive optical elements for the violet wavelength fabricated by electron-beam lithography. *Appl. Opt.* **41** (13) 2390-2393 (2002).
11. Sweeney, D. W. and Sommargren, G. E. Harmonic diffractive lenses. *Appl. Opt.* **34**(14), 2469-2475 (1995).

12. Faklis, D. and Morris, G. M. Spectral properties of multiorder diffractive lenses. *Appl. Opt.* **34**(14) 2462-2468 (1995).
13. Menon, R., Rogge, P. and Tsai, H-Y. Design of diffractive lenses that generate optical nulls without phase singularities. *J. Opt. Soc. Am. A*, **26**(2), 297 (2009).
14. Kim, G., Dominguez-Caballero, J-A. and Menon, R. Design and analysis of multi-wavelength diffractive optics. *Opt. Exp.* **20**(2), 2814-2823 (2012).
15. Menon, R. and Wang, P. Nanophotonic scattering structure. US Patent 8,953,239 (2015).
16. Mohammad, N., Meem, M., Wan, X. and Menon, R. Full-color, large area, transmissive holograms enabled by multi-level diffractive optics. *Sci. Rep.* **7**, 5789 (2018).
17. Kim, G., Dominguez-Caballero, J-A., Lee, H., Friedman, D. and Menon, R. Increased photovoltaic power output via diffractive spectrum separation. *Phys. Rev. Lett.* **110**, 123901 (2013).
18. Wang, P., Mohammad, N. and Menon, R. Chromatic-aberration-corrected diffractive lenses for ultra-broadband focusing. *Sci. Rep.* **6**, 21545 (2016).
19. Mohammad, N., Meem, M., Shen, B., Wang, P. and Menon, R. Broadband imaging with one planar diffractive lens. *Sci. Rep.* **8**, 2799 (2018).
20. Meem, M., Majumder, A. and Menon, R. Full-color video and still imaging using two flat lenses. *Opt. Exp.* **26**(21) 26866-26871 (2018).
21. Banerji, S., Chanana, A., Condori, H., Nahata, A. and Sensale-Rodriguez, B. Conference on Lasers and Electro-Optics, OSA Technical Digest (online) paper JW2A.76 (2018).
22. Yu, N., Genevet, P., Kats, M. A., Aieta, F., Tetienne, J. P., Capasso, F. and Gaburro, Z. Light Propagation with Phase Discontinuities: Generalized Laws of Reflection and Refraction. *Science* **334**, 333–337 (2011).

23. Arbabi, A., Horie, Y., Ball, A. J., Bagheri, M. and Faraon, A. Subwavelength-thick lenses with high numerical apertures and large efficiency based on high-contrast transmitarrays. *Nature Commun.* **6**, 7069 (2015).
24. Lalanne, P. and Chavel, P. Metalenses at visible wavelengths: past, present, perspectives. *Laser & Photonics Reviews* **11**(3), 1600295 (2017).
25. Chen, W. T., Zhu, A.Y., Sisler, J., Bharwani, Z. and Capasso, F. A Broadband achromatic polarization-insensitive metalens consisting of anisotropic nanostructures. *arXiv preprint arXiv:1810.05050* (2018).
26. Aieta, F., Genevet, P., Kats, M.A., Yu, N., Blanchard, R., Gaburro, Z. and Capasso, F. Polarization insensitive metalenses at visible wavelengths. *Nano Letts.* **12**(9), pp.4932-4936 (2012).
27. Chen, W. T., Zhu, A. Y., Sanjeev, V., Khorasaninejad, M., Shi, Z., Lee, E. and Capasso, F. A broadband achromatic metalens for focusing and imaging in the visible. *Nature Nanotechnology* **13**, 220 (2018).
28. Zhang, S., Soibel, A., Keo, S. A., Wilson, D., Rafol, B., Ting, D. Z., She, A., Gunapala S. D. and Capasso, F. Solid-immersion metalenses for infrared focal-plane arrays. *Appl. Phys. Lett.* **113**, 111104 (2018).
29. Liang, Y., Liu, H., Wang, F., Meng, H., Guo, J., Li, J. and Wei, Z. High-efficiency, near-diffraction limited, dielectric metasurface lenses based on crystalline titanium dioxide at visible wavelengths. *Nanomaterials* **8**, 288 (2018).
30. Palfinger, U., *et al*, R2R fabrication of freeform micro-optics. *Proc. SPIE* **10520**, Laser-based Micro- and Nanoprocessing XII, 105200J (14 March, 2018).

31. Khorasaninejad, M., Chen, W. T., Zhu, A. Y., Oh, J., Devlin, R.C., Rousso D. and Capasso, F. Multispectral chiral imaging with a metalens. *Nano Lett.* **16**(11), pp.4595-4560 (2016).
32. Shen, B., Wang, P., Polson, R. C. and Menon, R. An ultra-high efficiency Metamaterial Polarizer. *Optica* **1**(5) 356-360 (2014).
33. Arbabi, E., Kamali, S. M., Arbabi, A., and Faraon, A. Full-stokes imaging polarimetry using dielectric metasurfaces. *ACS Photonics* **5**(8) 3132-3140 (2018).
34. Shen, B., Wang, P., Polson, R. C. and Menon, R. An integrated-nanophotonic polarization beamsplitter with $2.4\mu\text{m} \times 2.4\mu\text{m}^2$ footprint. *Nature Photonics* **9**, 378-382 (2015).
35. Shen, B., Polson, R. C. and Menon, R. Increasing the density of integrated-photonic circuits via nanophotonic cloaking. *Nature Communications*. **7**, 13126 (2016).
36. Majumder, A., Shen, B., Polson, R. C. and Menon, R. Ultra-compact polarization rotation in integrated silicon photonics using digital metamaterials. *Opt. Exp.* **25**(17) 19721-19731 (2017).

Acknowledgements

We thank Tom Tiwald from Woollam for assistance with dispersion measurements, and Apratim Majumder for assistance with FDTD modeling. RM and MM acknowledge funding from Office of Naval Research (#N66001-10-1-4065). BSR and SB acknowledge support from NSF CAREER award: ECCS #1351389.

Author Contributions

SB performed the design and simulations. MM performed fabrication and analyzed the results. BSR provided design guidance and analyzed the results. RM provided design guidance and analyzed the results. All authors prepared and edited the manuscript.

Competing Interests Statement

RM is co-founder of Oblate Optics, Inc., which is commercializing technology discussed in this manuscript. The University of Utah has filed for patent protection for technology discussed in this manuscript.

Materials and Correspondence

Correspondence and materials requests should be addressed to RM at rmenon@eng.utah.edu.

Imaging with flat optics: metalenses or diffractive lenses?

Supplementary Information

Sourangsu Banerji,¹ Monjurul Meem,¹ Berardi Sensale-Rodriguez¹ and Rajesh Menon^{1,2,a)}

¹Department of Electrical and Computer Engineering, University of Utah, Salt Lake City, UT 84112, USA.

²Oblate Optics, Inc. 13060 Brixton Place, San Diego CA 92130, USA.

a) rmenon@eng.utah.edu

1. Literature Survey

A brief historical review of metalenses is necessary to appreciate its importance with relevance to its counterparts. The concept of such nanostructured sub-wavelength structures is not new. It actually dates back to year 1995-1996 [1-6], when the initial demonstrations of graded effective-index artificial-dielectrics for visible frequencies yielded very disappointing results with low measured diffraction efficiencies. The reasons for failure can be attributed to the following reasons. Firstly, the design assumed “adiabatic” effective index gradient [2, 4]. Secondly, improper understanding of the relation between local subwavelength gratings and artificial dielectrics [1-3]. Lastly, the modeling was challenging as it led to aspect ratios quite difficult to manufacture with the materials and patterning technologies, which operated during that time [5].

Fast-forward 15 years later, the field was again revived when a paper was published in Science that revisited Snell's law at the interface between two uniform media with the help of an ultrathin grating composed of metallic nano-antennas etched on the interface [7]. Shortly after this, another paper [8] was published which controlled the phase using the plasmonic dispersion inside a waveguiding slit in a metal which ultimately led to the focusing of the incident light beam. This was really an important result from the perspective that it showed that due to this resonance occurring at the interface, the phase delay is amplified in contrast to the propagation delay. Therefore, the constraint of having large aspect ratios can now be considerably relaxed. This possibility was already quite intuitive in the previous paper also; but was very subtle in the presentation to be noticed. The novelty, which underlined in both these two papers, was the fact that graded phases can now be implemented by carefully designed nano-structures specifically; nano-antennas.

To summarize, metalenses unprecedented success can be attributed to three main reasons. The first reason is that these metalenses can control the phase propagation delay through an effective-index modulation leading to a waveguiding effect of the transmitted wavefront. Secondly, these nanostructures can quite effectively also monitor the phase with graded sizes or orientations. Both the reasons combined provide the advantage to have fine spatial sampling with sub-wavelength "unit-cells"; thereby providing a rapid and robust spatial variation of the wrapped phase at the outer zones of the lens. Lastly, the introduction of a resonance delay (occurrence of a plasmonic resonance at the interface leading to amplified phase delay in contrast to the propagation delay) [9-12] to implement resonant high-contrast metalenses by combining two resonances, each covering a standard phase range of π [13-15]. This also relaxed the constraint on having stringent aspect ratios in the designed metalenses. Later on, it was also shown that by

using centrosymmetric or rotationally asymmetric structures, full wavefront control could be achieved with a Berry-phase vortex [16]. As an immediate result, many research groups across the world started demonstrating nanostructured metasurfaces having the ability to control the amplitude, phase, polarization, orbital momentum, absorption, reflectance, emissivity of light with high spatial resolution.

Following are some of the game changing publications in the area among many to have appeared in various reputed journals throughout the past decade and has been provided herein to give a perspective of how the field has evolved until today.

Table S1: Narrowband Metalenses (highlighted designs were used for comparison in Table 1 in main text).

Material	Wavelength	N.A.	Focal Length/ Diameter	Simulated Efficiency	Feature Width/Height	Polarization	Reference
c-Si	532 nm	0.98	5.1 μm / 50 μm	71%	20 nm / 500 nm	Circular	[17]
TiO ₂	405 nm	0.8	90 μm / 240 μm	86%	40 nm / 600 nm	Circular	[18]
TiO ₂	532 nm	0.8	90 μm / 240 μm	86%	40 nm / 600 nm	Circular	[18]
TiO ₂	532 nm	0.8	90 μm / 240 μm	86%	40 nm / 600 nm	Circular	[18]
TiO ₂	580 nm	0.94	200 μm / 1000 μm	79%	> 100 nm / 550 nm	Polarization Insensitive	[19]
a-Si	715 nm	0.99	42 μm / 600 μm	88%	50 nm / 250 nm	Linear	[20]
p-Si	550 nm	0.43	100 μm / 96 μm	38%	100 nm / 100 nm	Linear	[21]
TiO ₂	530 nm	0.2	67 μm / 26.4 μm	92%	50 nm / 600 nm	Polarization Insensitive	[22]
a-Si	1550 nm	0.97	25 μm / 100 μm	72%	200 nm / 950 nm	Circular	[10]
Au (gold)	1550 nm	0.015	3 cm / 0.9 mm	1%	50nm / 60 nm	Linear	[23]
Au (gold)	1550 nm	0.075	6 cm / 0.9 mm	1%	50nm / 60 nm	Linear	[23]
Au (gold)	676 nm	0.62	2.5 μm / 4 μm	~10%	30 nm / 30 nm	Linear	[24]
Au (gold)	676 nm	0.57	5 μm / 7 μm	~10%	30 nm / 30 nm	Linear	[24]
Au (gold)	676 nm	0.56	7 μm / 9.4 μm	~10%	30 nm / 30 nm	Linear	[24]

			um				
a-Si	850 nm	0.7	10 um / 20 um	93%	390 nm / 475 nm	Polarization Insensitive	[9]
c-Si	1060 nm	0.6	40 um / 60 um	89%	150 nm / 520 nm	Circular	[25]
Au (gold)	800 nm	-	5.7 um / 1.06 um	Qualitative Agreement	34 nm / 50 nm	Circular	[26]
Au (gold)	740 nm	-	10 um / 8 um	Qualitative Agreement	50 nm / 40 nm	Circular	[27]
TiO2	532 nm	0.6	200 um / 300 um	> 87%	250 nm / 600 nm	Polarization Insensitive	[28]
TiO2	405 nm	0.6	200 um / 300 um	> 87%	250 nm / 600 nm	Polarization Insensitive	[28]
TiO2	660 nm	0.6	200 um / 300 um	> 87%	250 nm / 600 nm	Polarization Insensitive	[28]
TiO2	532 nm	0.85	90 um / 300 um	83%	250 nm / 600 nm	Polarization Insensitive	[28]
TiO2	405 nm	0.85	90 um / 300 um	79%	250 nm / 600 nm	Polarization Insensitive	[28]
TiO2	660 nm	0.85	90 um / 300 um	84%	250 nm / 600 nm	Polarization Insensitive	[28]
a-Si	1550 nm	0.2	50 mm / 20 mm	> 90%	830 nm / 600mm	Polarization Insensitive	[29]
PbTe	5.2 um	-	5.2um / -	-	2500 nm / 650 nm	-	[30]
GaSb	4 um	0.36	155 um / ~300 um	80%	30 um / 2 um	Polarization Insensitive	[31]
a-Si	4 um	0.45	300 um / 300 um	~ 96%	600 nm / 2 um	Polarization Insensitive	[32]
a-Si	633 nm	1	633 nm / 30 um	2.50%	22 nm / 0.24 um	Linear	[33]
Si	473 nm	0.6294	10 um / -	21.13%	42 nm / 400 nm	-	[34]
Si	532 nm	0.6294	10 um / -	54.66%	67 nm / 400 nm	-	[34]
Si	632.8 nm	0.6294	10 um / -	31.49%	102 nm / 400 nm	-	[34]
Ag/Alumina/Ag	633 nm	-	2.2 um / 3.6 um	Qualitative Agreement	- / 1332 nm	Polarization Insensitive	[35]
Ag/Alumina/Ag	633 nm	-	1.9 um / 2.8 um	Qualitative Agreement	- / 851 nm	Polarization Insensitive	[35]
GaN	430 nm	0.22	110 um / 50 um	-	50 nm / 600 nm	Circular	[36]
GaN	532 nm	0.22	110 um / 50 um	-	70 nm / 600 nm	Circular	[36]
GaN	633 nm	0.22	110 um / 50 um	-	100 nm / 600 nm	Circular	[36]
Ag / TiO2	660 nm	-	1.4 um / -	-	- / 2.8 um	-	[37]
Ag/Alumina	830 nm	-	1.8 um / -	-	- / 2 um	-	[37]

TiO2	633 nm	0.37	500 um / 400 um	~ 100%	300 nm / 155 nm	-	[38]
TiO2	633 nm	0.89	100 um / 400 um	~ 100%	300 nm / 155 nm	-	[38]
Ag	365 nm	-	1 um / 1.8 um	-	10 nm to 20 nm / 200 nm	Linear	[39]
Al	365 nm	-	0.5 um / 1.8 um	-	10 nm to 20 nm / 200 nm	Linear	[39]
Ag	365 nm	-	0.5 um / 1.8 um	-	10 nm to 20 nm / 200 nm	Linear	[39]
PbTe	5.2 um	0.71	500 um / -	~ 80%	2500 nm / 650 nm	Linear	[40]
Au (gold)	600 nm	0.58 to 0.85	3 um, 5um, 7 um / 10 um	~20%	100 nm , 60 nm, 40 nm / 40 nm	Linear	[41]
Au (gold)	785 nm	0.58 to 0.85	3 um, 5um, 7 um / 10 um	~20%	100 nm , 60 nm, 40 nm / 40 nm	Linear	[41]
Au (gold)	980 nm	0.58 to 0.85	3 um, 5um, 7 um / 10 um	~20%	100 nm , 60 nm, 40 nm / 40 nm	Linear	[41]
a-Si	658 nm	0.3511	400 um / 300 um	Qualitative Agreement	- / 15 to 50 nm	Polarization Insensitive	[42]
Si3N4	633 nm	0.98	10 um / 100 um	Qualitative Agreement	- / 695 nm	Unpolarized	[43]
Si3N4	633 nm	0.78	4 mm / 1 cmm	Qualitative Agreement	- / 695 nm	Unpolarized	[43]
Ag (Silver)	1550 nm	-	10 um / 8 um	-	80 nm / 50 nm	Linear	[44]
TiO2	633 nm	upto 0.8	2 um to 14 um / 5.4 um	88.50%	10 nm - 150 nm / 488 nm	Polarization Insensitive	[45]
TiO2	450 nm	0.1	1 mm / -	-	320 nm / 90 nm	Polarization Insensitive	[46]
TiO2	532 nm	0.1	1 mm / -	-	320 nm / 90 nm	Polarization Insensitive	[46]
TiO2	633 nm	0.1	1 mm / -	-	320 nm / 90 nm	Polarization Insensitive	[46]
TiO2	800 nm	0.247	40 um / 20 um	99% (cylindrical lens)	90 nm - 200 nm / 250 nm	-	[47]

Table S2: Broadband Metalenses (highlighted designs were used for comparison in Table 1 in main text).

Material	Wavelength	Bandwidth	N.A.	Focal Length/ Diameter	Simulated Efficiency	Feature Width/Height	Polarization	Reference
a-Si	1.3 um - 1.65 um	350 nm	0.24	200 um / 100 um	-	100 nm / 1400 nm	Polarization Insensitive	[48]
a-Si	1.2 um - 1.65 um	450 nm	0.13	800 um / 200 um	-	100 nm / 800 nm	Polarization Insensitive	[48]
a-Si	1.2 um -	200 nm	0.88	30 um /	-	100 nm / 800	Polarization	[48]

	1.40 μm			100 μm		nm	Insensitive	
GaN	400 nm - 660 nm	260 nm	0.106	235 μm / 50 μm	average 40% (measured)	45 nm/800 nm	Circular	[49]
TiO ₂	460 nm - 700 nm	240 nm	0.2	67 μm / 26.4 μm		50 nm / 600 nm	Polarization Insensitive	[22]
a-Si	1300 nm - 1800 nm	500 nm	0.04	7.5 mm / 600 μm	24%, 22%, and 28%	75 nm / 600 nm	Linear	[50]
Au/SiO ₂ /Au	1.2 nm - 1.68 μm	480 nm	0.268	100 μm / 55.55 μm	12.44 % (measured)	40nm / 30 nm	Circular	[51]
Au/SiO ₂ /Au	1.2 nm - 1.68 μm	481 nm	0.217	-	8.4 % (measured)	40nm / 30 nm	Circular	[51]
Au/SiO ₂ /Au	1.2 nm - 1.68 μm	482 nm	0.324	-	8.56 % (measured)	40nm / 30 nm	Circular	[51]
TiO ₂	470 nm - 670 nm	200	0.2	63 μm / 25.2 μm	50%	80 nm / 600 nm	Circular	[52]
PbTe	5.11 μm - 5.29 μm	180 nm	0.5 mm / -	-	-	/ 650 nm	-	[30]
GaSb	3 μm - 5 μm	2 μm	0.35	155 μm / >300 μm	70%	30 μm / 2 μm	Polarization Insensitive	[31]
a-Si	5 μm - 8 μm	3 μm	0.35	30* λ / -	-	- / 1.5* λ	Polarization Insensitive	[53]
a-Si	3.7 μm - 4.2 μm	0.5 μm	0.45	300 μm / 300 μm	~ 96%	/ 2 μm	Polarization Insensitive	[32]
GaN	435 nm - 685 nm	250 nm	0.17	20 μm / 7 μm	50% - 78%	160nm or 240 nm / 400 nm	Linear	[54]
Photoresist (polymer-ZEP520A)	436 nm - 685 nm	250 nm	0.17	20 μm / 7 μm	50% - 78%	160nm or 240 nm / 400 nm	Linear	[54]
PbTe	5.11 μm - 5.29 μm	180 nm	-	0.5 mm / 1 mm	~ 75%	2500 nm / 650 nm	Linear	[40]
Au	532 nm - 1080 nm	548 nm	-	7 μm / 10 μm	~ 20%	100 nm , 60 nm, 40 nm / 40 nm	Linear	[55]
a-Si	470 nm - 658 nm	188 nm	0.3511	400 μm / 300 μm	Qualitative Agreement	- / 15 to 50 nm	Polarization Insensitive	[42]
TiO ₂	490 nm - 550 nm	60 nm	0.2	485 μm / 200 μm	Qualitative Agreement	varied / 180 nm	-	[56]
TiO ₂	560 nm - 800 nm	240 nm	upto 0.8	2 μm to 14 μm / 5.4 μm	> 50%	10 nm - 150 nm / 488 nm	Polarization Insensitive	[45]
fused Si	486 nm - 656 nm	170 nm	0.1	100 mm / 20 mm	-	1300 nm / 560 nm	Polarization Insensitive	[57]

2. Measured Dispersion of Photopolymer S1813

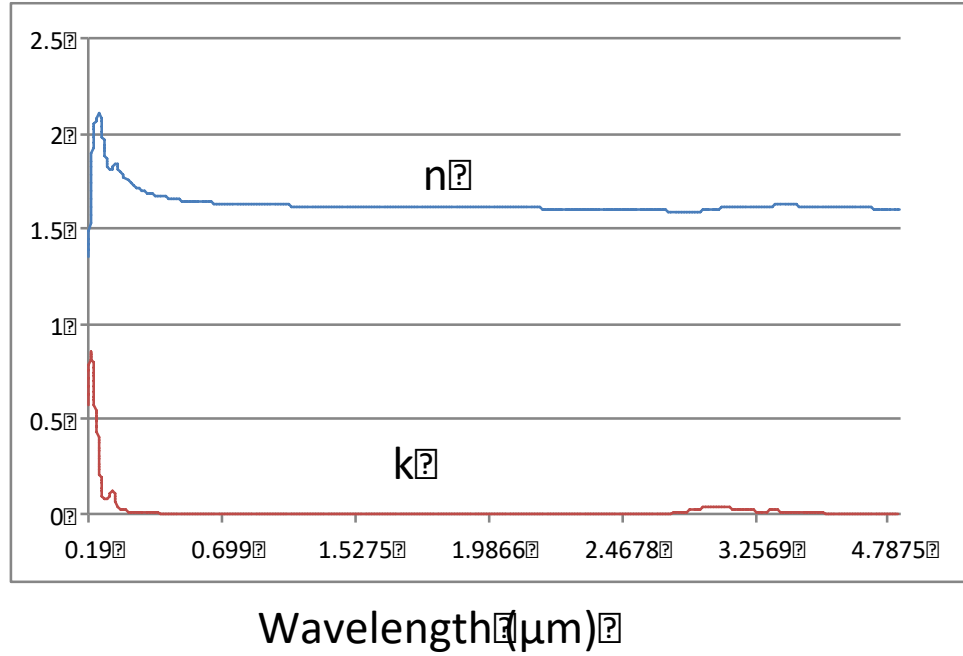


Figure S1: Measured dispersion of S1813.

3. FDTD Simulations

The full wave FDTD simulations were carried out using Lumerical FDTD Solutions. The material properties (refractive index and absorption coefficient as a function of frequency) of the Photoresist (S1813) was imported into Lumerical directly as the structure's optical data. A “.lsf” script was written to replicate the lens geometry using the same dimensions, which was specified during the optimization process as depicted in **Fig. S2 (a)**. An incident plane wave (type: diffracting [see [link](#)]) along the backward “y-axis” direction (with TM polarization) were used to illuminate the diffractive lens surface.

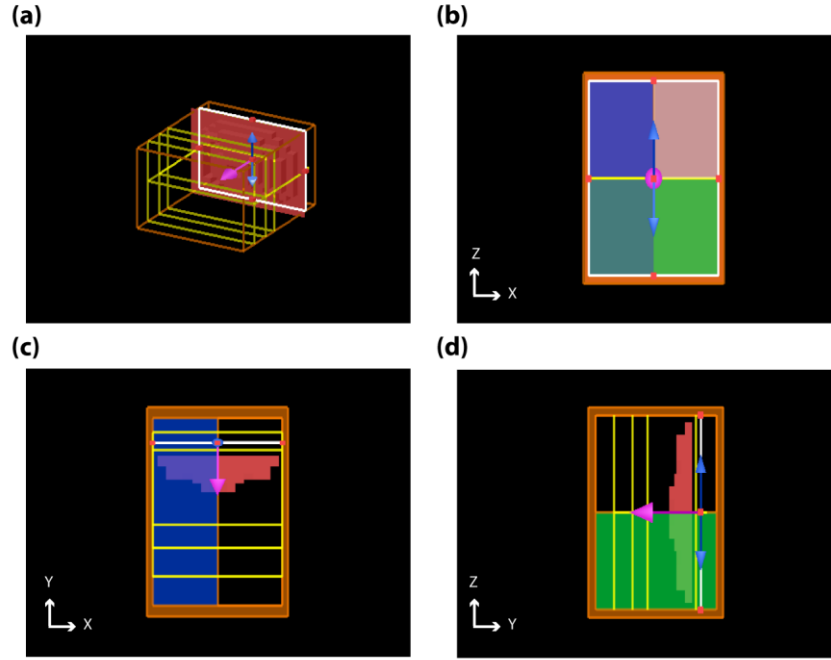


Figure S2 (a) Perspective view of the FDTD simulation setup of the spherical lens. (b) Visualization of boundary conditions imposed during the simulation. A boundary condition of (c) “symmetric” set to x-min and (d) “anti-symmetric” set to z-min.

For the broadband excitation, the entire range or bandwidth of the pulse was defined for the appropriate design. The entire FDTD simulation region was considered from the back surface of the spherical lens right up to 1.5 times the distance from the focal plane. A Perfectly Matched Layer (PML) boundary condition set up in the x-max, y-max and both z-min and z-max directions. As seen from **Fig. S2 (b-d)** that due to the inherent symmetry of the designed structure, the x-min boundary was set to “symmetric” and the z-min boundary was set to “anti-symmetric” which reduced the requirements by $\frac{1}{4}$ of the original simulation requirements in terms of both time and memory. We would like to emphasis here that we tried to impose radial symmetry but could not as it has not yet been made available in the software [see [link](#)].

The default mesh was used to simulate the structures instead of a very fine mesh to avoid the huge computation time. The mesh accuracy was kept at “3” which has a good tradeoff for precision and accuracy versus the time and memory requirement. Field monitors placed at different planes above the lens and along the vertical plane to observe the field profiles of the propagating electromagnetic radiation.

4. Methods of calculating focusing efficiency in selected metalens references

Reference 25 from main text: W. T. Chen, A.Y. Zhu, J. Sisler, Z. Bharwani, and F. Capasso, “A Broadband achromatic polarization-insensitive metalens consisting of anisotropic nanostructures,” arXiv preprint arXiv:1810.05050 (2018).

This paper does not explicitly define the focusing efficiency of the metalens.

Reference 26 from main text: F. Aieta, P. Genevet, P., M.A. Kats, N. Yu, R. Blanchard, Z. Gaburro, and F. Capasso, “Polarization insensitive metalenses at visible wavelengths,” Nano Letts, 12(9), pp.4932-4936 (2012).

This paper defines focusing efficiency as “the ratio of the optical power in the focal spot area (circle of radius $2 \times \text{FWM}$ spanning the center of the focal spot) to the incident optical power.”

We computed the focusing efficiency of the corresponding MDL with this definition and confirmed that the number (89.3%) was almost identical to the number with our definition in the main text (90%).

Reference 23 from main text: A. Arbabi, Y. Horie, A. J. Ball, M. Bagheri, and A. Faraon, “Subwavelength-thick lenses with high numerical apertures and large efficiency based on high-contrast transmitarrays,” Nature Commun. 6, 7069 (2015).

This paper defines focusing efficiency as the ratio of the optical power in an area of diameter $3 \times \text{FWHM}$ to the total incident power (which is the same as what we used).

Reference 27 from main text: W. T. Chen, A. Y. Zhu, V. Sanjeev, M. Khorasaninejad, Z. Shi, E. Lee, and F. Capasso, “A broadband achromatic metalens for focusing and imaging in the visible,” Nature Nanotechnology, 13, p.220 (2018).

This paper does not clearly define the definition of focusing efficiency. From the supplementary information, we can surmise that they are using the ratio of the power within the airy disk (which is approximately 2.5 times FWHM) to the total incident power.

Reference 28 from main text: S. Zhang, A. Soibel, S. A. Keo, D. Wilson, B. Rafol, D. Z. Ting, A. She, S. D. Gunapala and F. Capasso, “Solid-immersion metalenses for infrared focal-plane arrays,” Appl. Phys. Lett. 113, 111104 (2018).

This paper defines “The focusing efficiency was defined as the optical power over the pixel size of 10 μm at the focus divided by the incident power over the pixel pitch size of 30 μm .” This 10 μm corresponds to approximately 2 times FWHM of the middle wavelength (4 μm).

Reference 29 from main text: Y. Liang, H. Liu, F. Wang, F., H. Meng, J. Guo, J., J. Li, and Z. Wei, “High-efficiency, near-diffraction limited, dielectric metasurface lenses based on crystalline titanium dioxide at visible wavelengths,” Nanomaterials, 8, pp: 288 (2018).

From Fig. 6d of this paper, we estimate that the efficiency is defined as power within width of about 3 times FWHM divided by total incident power. The actual definition is not clearly stated.

5. Simulated Point Spread Functions (PSFs) [Broadband Lenses]

The simulated point spread functions (PSFs) for the broadband lenses designed at low, mid and high N.A. are provided.

Low NA Broadband Lens: [NA = 0.2 (470 nm – 670 nm)]

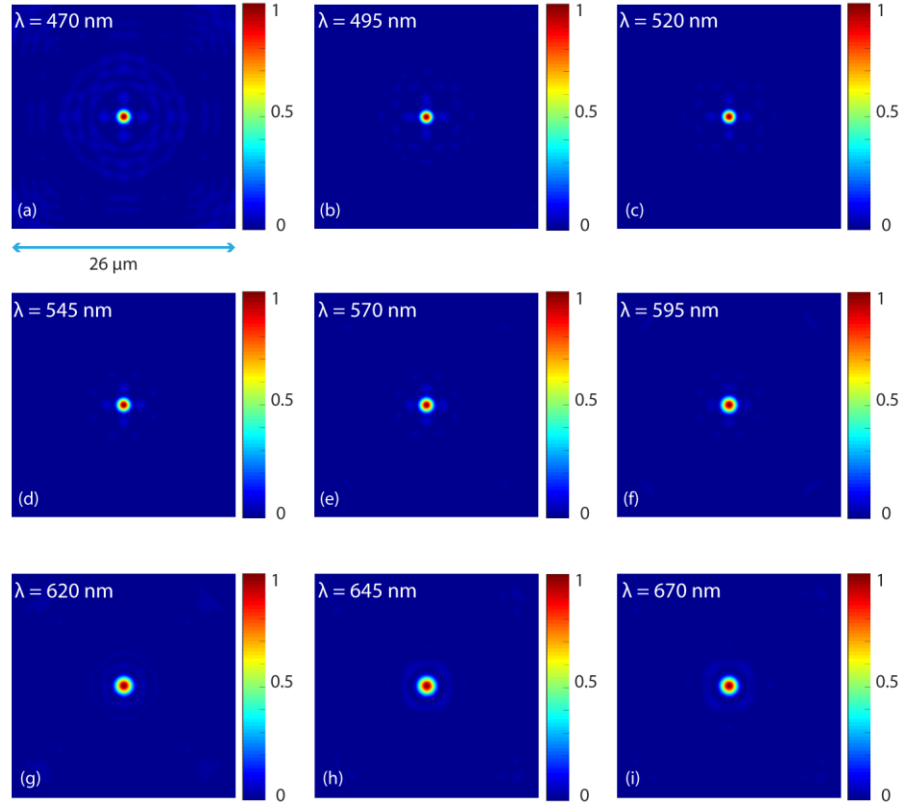


Figure S3 PSF plot corresponding to a wavelength of **(a)** 470 nm **(b)** 495 nm **(c)** 520 nm **(d)** 545 nm **(e)** 570 nm **(f)** 595 nm **(g)** 620 nm **(h)** 645 nm and **(i)** 670 nm.

Mid NA Broadband Lens: [NA = 0.36 (3 μm – 5 μm)]

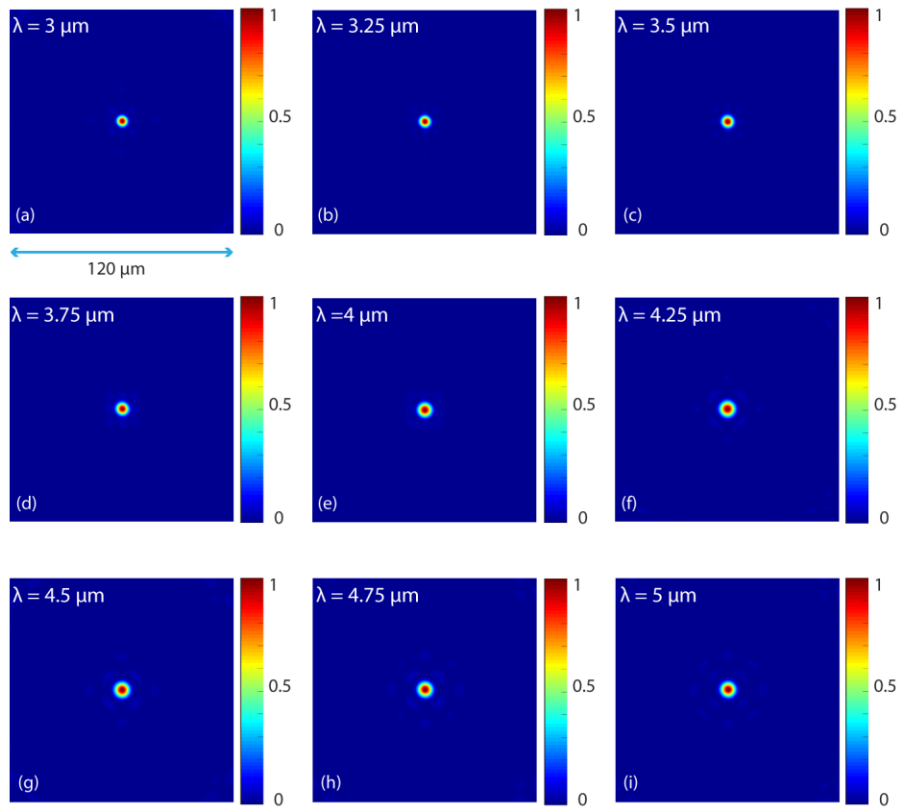


Figure S4 PSF plot corresponding to a wavelength of (a) 3 μm (b) 3.25 μm (c) 3.5 μm (d) 3.75 μm (e) 4 μm (f) 4.25 μm (g) 4.5 μm (h) 4.75 μm and (i) 5 μm .

High NA Broadband Lens: [NA = 0.81 (560 nm – 810 nm)]

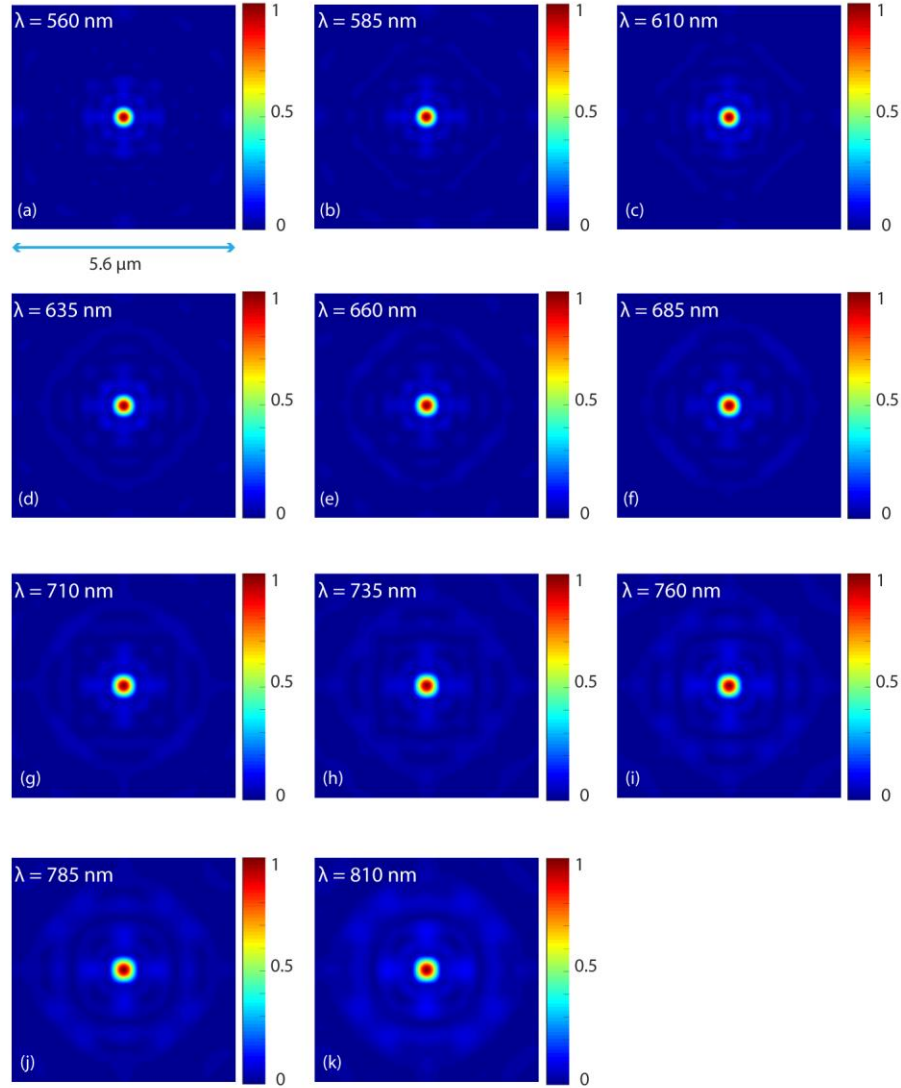


Figure S5 PSF plot corresponding to a wavelength of (a) 560 nm (b) 585 nm (c) 610 nm (d) 635 nm (e) 660 nm (f) 685 nm (g) 710 nm (h) 735 nm (i) 760 nm (j) 785 nm and (k) 810 nm.

6. Simulated FWHM and efficiency

Table S3: Low NA Narrowband Lens: [NA = 0.2 (530 nm)]

Wavelength (nm)	F.W.H.M. (Diffraction Limit) (μm)	F.W.H.M. (Simulation-FDTD) (μm)	Efficiency (%)
530	1.2956	1.2932	92.68

Table S4: Mid NA Narrowband Lens: [NA = 0.6 (532 nm)]

Wavelength (nm)	F.W.H.M. (Diffraction Limit) (um)	F.W.H.M. (Simulation-FDTD) (um)	Efficiency (%)
532	0.4433	0.5458	90.11

Table S5: High NA Narrowband Lens: [NA = 0.97 (1550 nm)]

Wavelength (nm)	F.W.H.M. (Diffraction Limit) (um)	F.W.H.M. (Simulation-FDTD) (um)	Efficiency (%)
1550	0.7986	0.8458	86.73

Table S6: Low NA Broadband Lens: [NA = 0.2 (470 nm – 670 nm)]

Wavelength (nm)	F.W.H.M. (Diffraction Limit) (um)	F.W.H.M. (Simulation-FDTD) (um)	Efficiency (%)
470	1.1628	1.1244	68.39
495	1.2247	1.1376	80.1
520	1.2865	1.1526	83.82
545	1.3484	1.2318	86.31
570	1.4103	1.3054	85.1
595	1.4721	1.454	81.35
620	1.534	1.5262	82.14
645	1.5958	1.5738	81.84
670	1.6577	1.5124	80.84

Table S7: Mid NA Broadband Lens: [NA = 0.36 (3 um – 5 um)]

Wavelength (um)	F.W.H.M. (Diffraction Limit) (um)	F.W.H.M. (Simulation-FDTD) (um)	Efficiency (%)
3	4.1552	4.218	80.43
3.25	4.5015	4.509	83.95
3.5	4.8477	4.821	90.93
3.75	5.194	5.086	90.88
4	5.5403	5.688	90.73
4.25	5.8865	6.124	85.09

4.5	6.2328	6.384	85.01
4.75	6.5791	5.977	84.73
5	6.9253	6.546	85.53

Table S8: High NA Broadband Lens: [NA = 0.81 (560 nm – 810 nm)]

Wavelength (nm)	F.W.H.M. (Diffraction Limit) (um)	F.W.H.M. (Simulation-FDTD) (um)	Efficiency (%)
560	0.3441	0.2912	71.73
585	0.3595	0.3645	71.32
610	0.3748	0.3578	69.22
635	0.3902	0.3945	73.46
660	0.4055	0.3952	74.03
685	0.4209	0.4104	71.69
710	0.4363	0.4134	69.5
735	0.4516	0.4278	67.73
760	0.467	0.4378	68.06
785	0.4823	0.4784	68.29
810	0.4977	0.4745	60.54

7. Aberrations Analysis

The Zernike polynomial coefficient was fitted over a circular shaped pupil. The calculation was done using the reference [57]. The fit was achieved with a least squares fit method. The indexing scheme used was Fringe.

Table S9: Aberrations coefficients

Radial degree (n)	Azimuthal degree (m)	Fringe index (j)	Classical name
0	0	1	piston
1	1	2	tip
1	-1	3	tilt
2	0	4	defocus
2	2	5	vertical astigmatism
2	-2	6	oblique astigmatism

3	1	7	horizontal coma
3	-1	8	vertical coma
4	0	9	primary spherical
3	3	10	oblique trefoil
3	-3	11	vertical trefoil
4	2	12	vertical secondary astigmatism
4	-2	13	oblique secondary astigmatism
4	4	14	vertical quadrafoil
4	-4	15	oblique quadrafoil

The following lists all the fitting coefficients for the designed lenses:

Table S10: Low NA Narrowband Lens: [NA = 0.2 (530 nm)]

Wavelength (nm)	Piston	Tip	Tilt	Defocus	Vertical astigmatism	Oblique astigmatism	Horizontal coma	Vertical coma	Primary spherical	Oblique trefoil	Vertical trefoil	Vertical secondary astigmatism	Oblique secondary astigmatism	Vertical quadrafoil	Oblique quadrafoil
530	4.27E-03	-4.90E-20	1.03E-20	-0.009314435145	-1.39E-19	-1.72E-21	-9.63E-21	1.19E-20	0.01542385988	1.79E-19	-2.64E-21	8.38E-20	-6.65E-21	2.25E-04	8.12E-21

Table S11: Mid NA Narrowband Lens: [NA = 0.6 (532 nm)]

Wavelength (nm)	Piston	Tip	Tilt	Defocus	Vertical astigmatism	Oblique astigmatism	Horizontal coma	Vertical coma	Primary spherical	Oblique trefoil	Vertical trefoil	Vertical secondary astigmatism	Oblique secondary astigmatism	Vertical quadrafoil	Oblique quadrafoil
532	1.64E-04	-5.78E-20	6.19E-21	5.70E-05	1.12E-19	5.07E-21	4.55E-20	6.73E-21	7.97E-05	1.74E-20	3.16E-20	-7.17E-20	5.45E-21	-9.13E-08	8.18E-22

Table S12: High NA Narrowband Lens: [NA = 0.97 (1550 nm)]

Wavelength (nm)	Piston	Tip	Tilt	Defocus	Vertical astigmatism	Oblique astigmatism	Horizontal coma	Vertical coma	Primary spherical	Oblique trefoil	Vertical trefoil	Vertical secondary astigmatism	Oblique secondary astigmatism	Vertical quadrafoil	Oblique quadrafoil
1550	3.53E-05	-6.89E-22	-1.77E-22	-8.78E-05	5.78E-21	1.56E-22	7.21E-22	6.07E-22	0.0001360991827	4.66E-22	2.51E-23	-1.39E-21	2.86E-22	1.93E-08	5.05E-23

Table S13: Low NA Broadband Lens: [NA = 0.2 (470 nm – 670 nm)]

Wavelength (nm)	Piston	Tip	Tilt	Defocus	Vertical astigmatism	Oblique astigmatism	Horizontal coma	Vertical coma	Primary spherical	Oblique trefoil	Vertical trefoil	Vertical secondary	Oblique secondary	Vertical quadrafoil	Oblique quadrafoil
-----------------	--------	-----	------	---------	----------------------	---------------------	-----------------	---------------	-------------------	-----------------	------------------	--------------------	-------------------	---------------------	--------------------

										l	l	astigma tism	astigma tism		foil
470	1.49 E- 02	- 6.67 E- 19	- 8.83 E- 21	- 0.0164895 5077	2.78E- 18	2.16E- 21	5.41E -19	5.00 E-20	0.0179052 6432	6.14 E-19	- 6.00 E-20	8.05E- 18	3.07E- 20	- 0.00160488 0073	2.79E -21
495	7.24 E- 03	- 1.40 E- 19	9.34 E- 22	- 0.0118985 7301	-3.11E- 19	-2.29E- 21	3.18E -21	- 1.06 E-20	0.0162798 5935	3.60 E-19	1.59 E-20	-8.59E- 19	1.77E- 20	- 0.00070758 70624	7.38E -21
520	6.11 E- 03	- 2.23 E- 19	- 3.93 E- 21	- 0.0109625 027	1.02E- 19	-1.69E- 20	- 2.21E -19	1.25 E-20	0.0172054 3958	3.88 E-19	- 1.53 E-20	-2.41E- 19	-1.09E- 20	- 0.00161376 52	- 1.40E -20
545	5.76 E- 03	- 1.15 E- 19	- 5.19 E- 21	- 0.0103661 4896	-4.39E- 19	2.67E- 20	2.70E -19	- 4.25 E-20	0.0182571 2339	9.85 E-20	8.80 E-21	-9.94E- 20	-1.33E- 19	- 0.00244872 8824	3.77E -20
570	6.34 E- 03	8.19 E- 20	- 6.06 E- 20	- 0.0109036 6043	4.00E- 19	-4.77E- 20	2.23E -19	6.43 E-20	0.0199512 6743	2.57 E-19	- 6.13 E-21	-1.95E- 19	9.59E- 20	- 0.00292379 7378	- 2.40E -20
595	7.23 E- 03	1.45 E- 19	- 2.95 E- 20	- 0.0124356 7048	-2.38E- 19	1.33E- 19	2.85E -19	- 2.24 E-20	0.0219853 4022	3.46 E-19	- 7.70 E-20	8.89E- 19	1.76E- 19	- 0.00239573 4023	0.00E +00
620	8.84 E- 03	- 4.90 E- 19	4.73 E- 21	- 0.0158614 715	5.30E- 19	4.06E- 20	5.99E -20	2.01 E-20	0.0265758 3541	2.47 E-19	5.35 E-20	-1.19E- 19	-2.99E- 20	- 0.00327783 9978	- 1.50E -20
645	8.87 E- 03	- 3.64 E- 19	- 2.47 E- 20	- 0.0174448 9829	5.92E- 19	1.12E- 19	1.46E -19	2.80 E-20	0.0267463 5366	2.74 E-19	1.05 E-20	4.07E- 21	7.82E- 21	- 0.00261779 9596	2.74E -20
670	8.42 E- 03	- 3.36 E- 20	7.69 E- 21	- 0.0172334 0287	-1.85E- 19	-3.14E- 21	2.14E -19	3.99 E-20	0.0255197 3278	5.14 E-19	4.35 E-20	-1.21E- 18	-1.22E- 20	- 0.00204955 599	- 1.22E -20

Table S14: Mid NA Broadband Lens: [NA = 0.36 (3 μ m – 5 μ m)]

Wavele ngth (nm)	Pist on	Tip	Tilt	Defocus	Vertica l astigma tism	Obliqu e astigma tism	Horizontal coma	Verti cal com a	Primary spherical	Obli que trefo il	Verti cal trefo il	Vertica l second ary astigma tism	Obliqu e second ary astigma tism	Vertical quadrafoil	Obliq ue quadr afoil
3	5.2 4E- 03	- 4.2 6E- 05	4.2 6E- 05	- 0.0062821 94933	4.12E- 19	- 1.26E- 20	- 0.0003431 500251	3.43 E- 04	0.013538 79275	- 9.87 E- 05	- 9.87 E- 05	- 1.10E- 19	- 3.24E- 20	0.0015691 26352	3.24E -20
3.25	4.6 4E- 03	- 1.7 5E- 05	1.7 5E- 05	- 0.0069560 88722	1.21E- 19	- 6.74E- 21	- 0.0003399 400209	3.40 E- 04	0.013017 48094	- 5.13 E- 05	- 5.13 E- 05	2.25E- 19	8.70E- 21	0.0006576 337018	9.57E -20
3.5	4.7 3E- 03	- 1.7 3E- 05	1.7 3E- 05	- 0.0075514 73879	6.99E- 20	- 1.16E- 19	- 0.0003880 635223	3.88 E- 04	0.013593 57705	- 1.16 E- 05	- 1.16 E- 05	1.42E- 19	1.03E- 19	0.0007015 665668	- 1.87E -20
3.75	5.2 2E- 03	1.3 2E- 05	- 1.3 2E-	- 0.0089255 15569	4.38E- 19	- 3.89E- 21	- 0.0004279 703352	4.28 E- 04	0.015194 48031	- 1.04 E-	- 1.04 E-	3.56E- 20	5.03E- 21	0.0007907 630242	1.51E -20

			05							05	05				
4	6.1 5E- 03	4.0 1E- 05	- 4.0 1E- 05	- 0.0108158 1694	- 5.08E- 20	- 5.99E- 20	- -2.11E-04	2.11 E- 04	0.017385 2022	- 1.33 E- 05	- 1.33 E- 05	9.19E- 20	1.60E- 20	0.0010037 89483	1.60E -20
4.25	7.1 5E- 03	6.7 7E- 05	- 6.7 7E- 05	- 0.0119973 7678	3.20E- 19	- 8.81E- 21	-2.13E-04	2.13 E- 04	0.020153 83329	- 3.23 E- 05	- 3.23 E- 05	- 7.74E- 20	- 5.69E- 21	0.0011998 22716	- 3.41E -20
4.5	7.1 4E- 03	8.8 1E- 05	- 8.8 1E- 05	- 0.0123777 8106	- 5.92E- 20	- 3.75E- 20	-2.00E-04	2.00 E- 04	0.021764 61854	1.22 E- 05	1.22 E- 05	1.30E- 20	- 1.82E- 20	0.0011773 27913	6.05E -21
4.75	6.6 9E- 03	3.9 5E- 05	- 3.9 5E- 05	- 0.0126660 3737	- 2.20E- 20	- 2.23E- 20	- 0.0003298 267573	3.30 E- 04	0.022327 16133	- 4.99 E- 05	- 4.99 E- 05	1.79E- 20	3.20E- 20	0.0009656 442358	- 4.80E -20
5	6.7 2E- 03	1.1 3E- 05	- 1.1 3E- 05	- 0.0125685 5892	- 1.01E- 20	- 2.08E- 20	- 0.0004088 105373	4.09 E- 04	0.022347 37438	- 4.58 E- 05	- 4.58 E- 05	- 6.55E- 20	6.05E- 20	0.0004061 059614	9.41E -20

Table S15: High NA Broadband Lens: [NA = 0.81 (560 nm – 810 nm)]

Wavele ngth (nm)	Pist on	Tip	Tilt	Defocus	Vertica l astigma tism	Obliqu e astigma tism	Horizo ntal coma	Vertic al coma	Primary spherical	Obli que trefoi l	Vertic al trefoil	Vertica l second ary astigma tism	Obliqu e second ary astigma tism	Vertical quadrafoil	Obliqu e quadra foil
560	1.8 5E- 02	1.8 4E- 19	- 6.75E -20	- 0.024760 71025	3.10E- 19	8.26E- 20	2.04E -19	9.55E -20	0.040656 20221	1.65 E- 18	- 4.77E -20	5.20E- 19	2.13E- 19	0.0040490 14203	0.00E +00
585	1.8 6E- 02	- 2.6 0E- 20	0.00E +00	- 0.025344 8257	1.11E- 18	8.65E- 20	6.55E -19	1.00E -19	0.038980 29116	1.69 E- 18	0	- 7.25E- 19	- 1.12E- 19	0.0050142 91195	2.23E -19
610	1.8 7E- 02	2.0 0E- 19	- 7.39E -20	- 0.028762 55086	5.03E- 19	0.00E +00	3.82E -19	0.00E +00	0.038212 77303	1.84 E- 18	- 5.23E -20	- 4.30E- 19	0.00E +00	0.0026347 13919	- 1.75E -19
635	2.0 1E- 02	5.1 2E- 19	- 3.84E -20	- 0.029578 44367	- 1.22E- 18	9.39E- 20	2.96E -19	1.63E -19	0.036954 33521	1.48 E- 18	- 5.43E -20	4.45E- 19	1.21E- 19	0.0004871 430698	6.06E -20
660	2.1 1E- 02	- 4.3 6E- 19	0.00E +00	- 0.030394 7465	- 2.50E- 19	9.78E- 20	9.45E -19	0.00E +00	0.034618 92415	1.03 E- 18	1.13E -19	1.94E- 19	0.00E +00	7.96E-05	0.00E +00
685	2.1 6E- 02	- 5.6 1E- 19	- 2.08E -20	- 0.032665 87241	2.97E- 18	7.66E- 20	7.65E -19	1.18E -19	0.031866 84042	1.38 E- 18	5.90E -20	- 5.48E- 19	0.00E +00	1.64E-04	1.65E -19
710	2.4 6E- 02	7.7 0E- 19	- 1.29E -19	- 0.033940 94395	- 1.25E- 19	0.00E +00	1.16E -18	0.00E +00	0.032888 78716	1.77 E- 18	- 1.22E -19	- 2.31E- 18	- 1.36E- 19	0.0026186 02593	6.80E -20
735	2.7 7E- 02	- 1.5 0E- 18	4.50E -20	- 0.034818 05191	1.53E- 18	5.51E- 20	7.64E -19	1.27E -19	0.030481 89555	2.04 E- 18	- 1.91E -19	1.30E- 19	- 1.42E- 19	0.0052473 69014	1.42E -19
760	3.0 5E- 02	- 2.9	- 1.17E	- 0.038873	- 7.91E-	2.29E- 19	1.70E -18	3.31E -20	0.030349 68533	2.53 E-	- 6.61E	- 8.62E-	- 2.96E-	0.0031198 67851	7.38E -20

	02	6E-21	-19	01251	19					18	-20	19	19		
785	3.3 1E-02	- 1.2 5E-18	0.00E +00	- 0.040368 00884	3.11E- 18	0	2.84E -18	1.35E -19	0.027858 44987	1.61 E-18	- 6.77E -20	- 8.63E- 19	- 2.27E- 19	0.0014933 26151	1.51E -19
810	4.2 3E-02	- 4.2 1E-19	4.96E -20	- 0.045632 54646	- 2.68E- 18	6.08E- 20	1.90E -18	2.11E -19	0.022121 67989	3.57 E-18	0.00E +00	- 1.88E- 18	7.85E- 20	0.0007521 237151	0.00E +00

References

1. F. T. Chen and H. G. Craighead, "Diffractive phase elements based on two-dimensional artificial dielectrics." Opt. Lett. 20, 121–123 (1995).
2. Z. Zhou and T. J. Drabik, "Optimized binary, phase-only, diffractive optical element with subwavelength features for 1.55 μm ." J. Opt. Soc. Am. A 12, 1104–1112 (1995).
3. J. M. Miller, N. de Beaucoudrey, P. Chavel, E. Cambril, and H. Launois, "Synthesis of a subwavelength-pulse-width spatially modulated array illuminator for 0.633 μm ." Opt. Lett. 21, 1399–1401 (1996).
4. F. T. Chen and H. G. Craighead, "Diffractive lens fabricated with mostly zeroth-order gratings." Opt. Lett. 21, 177–179 (1996).
5. M. E. Warren, R. E. Smith, G. A. Vawter, and J. R. Wendt, "High-efficiency subwavelength diffractive optical element in GaAs for 975 nm." Opt. Lett. 20, 1441–1443 (1996)
6. M. T. Gale, "Replication techniques for diffractive optical elements." Microelectr. Eng. 34, 321–339 (1997).
7. N. Yu, P. Genevet, M. A. Kats, F. Aieta, J. P. Tetienne, F. Capasso, and Z. Gaburro, "Light propagation with phase discontinuities: generalized laws of reflection and refraction." Science 334, 333–337 (2011).
8. S. Ishii, A. V. Kildishev, V. M. Shalaev, K. P. Chen, and V.P. Drachev, "Metal nanoslit lenses with polarization-selective design." Opt. Lett. 36, 451–453 (2011).

9. S. Vo, D. Fattal, W. V. Sorin, Z. Peng, T. Tran, M. Fiorentino, and R. G. Beausoleil, "Sub-wavelength grating lenses with a twist." *IEEE Photon. Technol. Lett.* 26, 1375–78 (2014).
10. A. Arbabi, Y. Horie, A. J. Ball, M. Bagheri, and A. Faraon, "Subwavelength-thick lenses with high numerical apertures and large efficiency based on high-contrast transmitarrays." *Nature Commun.* 6, 7069 (2015).
11. Y. F. Yu, A. Y. Zhu, R. Paniagua-Dominguez, Y. H. Fu, B. Luk'yanchuk, and A. I. Kuznetsov, "High-transmission dielectric metasurface with 2π phase control at visible wavelengths" *Laser Photonics Rev.* 9, 412–418 (2015).
12. M. Decker, I. Staude, M. Falkner, J. Dominguez, D. N. Neshev, I. Brener, T. Pertsch, and Y. S. Kivshar, "High-efficiency dielectric Huygens' surfaces." *Adv. Opt. Mat.* 3, 813–820 (2015)
13. A. Arbabi, E. Arbabi, S. M. Kamali, Y. Horie, S. Han, and A. Faraon, "Miniature optical planar camera based on a wide-angle metasurface doublet corrected for monochromatic aberrations." *Nat. Commun.* 7, 13682 (2016).
14. M. Khorasaninejad, Z. Shi, A. Y. Zhu, W. T. Chen, V. Sanjeev, A. Zaidi, and F. Capasso, "Achromatic metalens over 60 nm bandwidth in the visible and metalens with reverse chromatic dispersion." *Nano Lett.* 17, 1819–1824 (2017).
15. K. Li, Y. Guo, M. Pu, X. Li, X. Ma, Z. Zhao, and X. Luo, "Dispersion controlling meta-lens at visible frequency." *Opt. Exp.* 25, 21419–21427 (2017).
16. E. Hasman, V. Kleiner, G. Biener, and A. Niv, "Polarization dependent focusing lens by use of quantized Pancharatnam–Berry phase diffractive optics." *Appl. Phys. Lett.* 82, 328 (2003).

17. H. Liang, Q. Lin, X. Xie, Q. Sun, Y. Wang, L. Zhou, L. Liu, X. Yu, J. Zhou, T. F. Krauss, and J. Li, "Ultrahigh Numerical Aperture Metalens at Visible Wavelengths" *Nano Lett.* 18, 4460 (2018).
18. W. T. Chen, A.Y. Zhu, M. Khorasaninejad, Z. Shi, V. Sanjeev, and F. Capasso, "Immersion meta-lenses at visible wavelengths for nanoscale imaging." *Nano. Lett.*, 17(5), pp.3188-3194 (2017)
19. S. J. Byrnes, A. Lenef, F. Aieta, F. and F. Capasso, "Designing large, high-efficiency, high-numerical-aperture, transmissive meta-lenses for visible light." *Opt. Exp.* 24(5), pp.5110-5124 (2016).
20. R. Paniagua-Dominguez, Y.F. Yu, E. Khaidarov, S. Choi, V. Leong, R.M. Bakker, X. Liang, Y. H. Fu, V. Valuckas, L.A. Krivitsky, A.I. and Kuznetsov, "A metalens with a near-unity numerical aperture." *Nano. Lett.*, 18(3), pp.2124-2132 (2018).
21. D. Lin, P. Fan, E. Hasman and M.L. Brongersma, "Dielectric gradient metasurface optical elements." *Science*, 345(6194), pp.298-302 (2014).
22. W. T. Chen, A.Y. Zhu, J. Sisler, Z. Bharwani, and F. Capasso, "A broadband achromatic polarization-insensitive metalens consisting of anisotropic nanostructures." *arXiv preprint arXiv:1810.05050* (2018).
23. F. Aieta, P. Genevet, M.A. Kats, N. Yu, R. Blanchard, Z. Gaburro, Z. and F. Capasso, "Aberration-free ultrathin flat lenses and axicons at telecom wavelengths based on plasmonic metasurfaces." *Nano Lett.*, 12(9), pp.4932-4936 (2012).
24. X. Ni, S. Ishii, A.V. Kildishev, and V.M. Shalaev, "Ultra-thin, planar, Babinet-inverted plasmonic metalenses." *Light: Science & Applications*, 2(4), p.e72 (2013).

25. Y. Qiu, H. Liang, J. Li, J., Wang, T.F. Krauss, and Z. Cai, "Efficient crystalline Silicon planar metalens towards fiber optical tweezers." In Asia Communications and Photonics Conference (pp. Su1F-5) (2017).
26. T. Roy, E.T. Rogers, and N.I. Zheludev, "Sub-wavelength focusing meta-lens." *Opt. Exp.*, 21(6), pp.7577-7582 (2013).
27. X. Chen, L. Huang, L., H. Mühlenbernd, G. Li, B. Bai, Q. Tan, G. Jin, C.W. Qiu, S. Zhang, and T. Zentgraf, "Dual-polarity plasmonic metalens for visible light." *Nat. comm.*, 3, p.1198 (2012).
28. M. Khorasaninejad, A.Y. Zhu, C. Roques-Carmes, W.T. Chen, J. Oh, I. Mishra, R.C. Devlin, and F. Capasso, "Polarization-insensitive metalenses at visible wavelengths." *Nano let.*, 16(11), pp.7229-7234 (2016).
29. A. She, S. Zhang, S. Shian, D.R. Clarke, and F. Capasso, "Large area metalenses: design, characterization, and mass manufacturing." *Opt. exp.*, 26(2), pp.1573-1585 (2018).
30. H. Zheng, J. Ding, L. Zhang, H. Lin, S. An, T. Gu, H. Zhang, and J. Hu, "Ultra-thin, high-efficiency mid-infrared Huygens metasurface optics." In 2018 International Applied Computational Electromagnetics Society Symposium (ACES) (pp. 1-2). IEEE (2018).
31. S. Zhang, A. Soibel, S.A. Keo, D. Wilson, S. Rafol, D.Z. Ting, A. She, S.D. Gunapala, and F. Capasso, "Solid-Immersion Metalenses for Infrared Focal Plane Arrays." *arXiv preprint arXiv:1805.06608* (2018).
32. H. Zuo, D.Y. Choi, X. Gai, P. Ma, L. Xu, D.N. Neshev, B. Zhang, and B. Luther-Davies, "High-Efficiency All-Dielectric Metalenses for Mid-Infrared Imaging." *Adv. Opt. Mat.*, 5(23), p.1700585 (2017).

33. V. V. Kotlyar, A.G. Nalimov, S.S. Stafeev, C. Hu, L. O’Faolain, M.V. Kotlyar, D. Gibson, and S. Song, “Thin high numerical aperture metalens.” *Opt. exp.*, 25(7), pp.8158-8167 (2017).
34. K. Li, Y. Guo, M. Pu, X. Li, X. Ma, Z. Zhao, and X. Luo, “Dispersion controlling meta-lens at visible frequency.” *Opt. exp.*, 25(18), pp.21419-21427 (2017).
35. C. Ma, and Z. Liu, “Designing super-resolution metalenses by the combination of metamaterials and nanoscale plasmonic waveguide couplers.” *Jour. of Nanophot.*, 5(1), p.051604 (2011).
36. B.H. Chen, P.C. Wu, V.C. Su, Y.C. Lai, C.H. Chu, I.C. Lee, J.W. Chen, Y.H. Chen, Y.C. Lan, C.H. Kuan, and D.P. Tsai, “GaN metalens for pixel-level full-color routing at visible light.” *Nano lett.* 17(10), pp.6345-6352 (2017).
37. C. Ma, M.A. Escobar, and Z. Liu, “Extraordinary light focusing and Fourier transform properties of gradient-index metalenses.” *Phys. Rev. B*, 84(19), p.195142 (2011).
38. H. Cai, D.A. Czaplewski, L. Stan, and D. López, “High-efficiency, low-aspect-ratio planar lens based on Huygens resonators.” In *Optical MEMS and Nanophotonics (OMN)*, 2017 International Conference on (pp. 1-2). IEEE (2017).
39. C. Ma, and Z. Liu, “A super resolution metalens with phase compensation mechanism.” *Appl. Phy. Lett.*, 96(18), p.183103 (2010).
40. L. Zhang, J. Ding, H. Zheng, S. An, H. Lin, B. Zheng, Q. Du, G. Yin, J. Michon, Y. Zhang, and Z. Fang, “Ultra-thin high-efficiency mid-infrared transmissive Huygens meta-optics.” *Nat. comm.*, 9(1), p.1481 (2018).
41. J. Hu, C.H. Liu, X. Ren, L.J. Lauhon, and T.W. Odom, “Plasmonic lattice lenses for multiwavelength achromatic focusing.” *ACS nano*, 10(11), pp.10275-10282 (2016).

42. H. C. Wang, C.H. Chu, P.C. Wu, H. H. Hsiao, H.J. Wu, J.-W. Chen, W.H. Lee, Y. C. Lai, Y. W Huang, M.L. Tseng, S. W. Chang, D.P. Tsai, “Ultrathin Planar Cavity Metasurfaces” *Small*, 14, 1703920 (2018).
43. Z.B. Fan, Z.K. Shao, M.Y. Xie, X.N. Pang, W.S. Ruan, F.L. Zhao, Y.J. Chen, S.Y. Yu. and J.W. Dong, “Silicon nitride metalenses for unpolarized high-NA visible imaging.” In *CLEO: Science and Innovations* (pp. STh3I-8) (2018).
44. Q. Sun, Q. Wang, S. Wang, and N. Ruan, “Planar metalens realizing subwavelength focusing.” In *2015 International Conference on Optical Instruments and Technology: Micro/Nano Photonics and Fabrication* (Vol. 9624, p. 962404) (2015).
45. Y. Liang, H. Liu, F. Wang, H. Meng, J. Guo, J. Li, and Z. Wei, “High-Efficiency, Near-Diffraction Limited, Dielectric Metasurface Lenses Based on Crystalline Titanium Dioxide at Visible Wavelengths” *Nanomaterials*, 8(5) (2018).
46. H. Cai, D. Czanlewski, K. Ozando, A. Martinson, D. Gosztola, L. Stan, and D. López, “Digitally Designed Ultrathin Metasurfaces for Multiwavelength Optics in the Visible.” In *2018 International Conference on Optical MEMS and Nanophotonics (OMN)* (pp. 1-2). IEEE (2018).
47. J. Ha, A. Ndao, L. Y. Hsu, J. H. Park, and B. Kanté, “All dielectric metasurface cylindrical lens,” *arXiv:1804.02356* (2018).
48. S. Shrestha, A. Overvig, M. Lu, A. Stein, N. Yu, “Broadband achromatic dielectric metalenses” *Light: Sci. Appl.* 2018, 7, 85.
49. S. Wang, P.C. Wu, V.C. Su, Y.C. Lai, M.K. Chen, H.Y. Kuo, B.H. Chen, Y.H. Chen, T.T. Huang, J.H. Wang, and R.M. Lin, “A broadband achromatic metalens in the visible.” *Nat. Nano.*, 13(3), p.227 (2018).

50. M. Khorasaninejad, F. Aieta, P. Kanhaiya, M.A. Kats, P. Genevet, D. Rousso, and F. Capasso, "Achromatic metasurface lens at telecommunication wavelengths." *Nano lett.* 15(8), pp.5358-5362 (2015).
51. S. Wang, P.C. Wu, V.C. Su, Y.C. Lai, C.H. Chu, J.W. Chen, S.H. Lu, J. Chen, B. Xu, C.H. Kuan, and T. Li, "Broadband achromatic optical metasurface devices." *Nat. comm.*, 8(1), p.187 (2017).
52. W.T. Chen, A.Y. Zhu, V. Sanjeev, M. Khorasaninejad, Z. Shi, E. Lee, and F. Capasso, "A broadband achromatic metalens for focusing and imaging in the visible." *Nat. Nano.*, 13(3), p.220 (2018).
53. Z. Lin, B. Groever, F. Capasso, A.W. Rodriguez, and M. Lončar, "Topology-Optimized Multilayered Metaoptics." *Phys. Rev. Appl.*, 9(4), p.044030 (2018).
54. M. Ye, V. Ray, and Y.S. Yi, "Achromatic Flat Subwavelength Grating Lens Over Whole Visible Bandwidths." *IEEE Phot. Tech. Lett.*, 30(10), pp.955-958 (2018).
55. J. Hu, C.H. Liu, X. Ren, L.J. Lauhon, and T.W. Odom, "Plasmonic lattice lenses for multiwavelength achromatic focusing." *ACS nano*, 10(11), pp.10275-10282 (2016).
56. Z. Shi, M. Khorasaninejad, A.Y. Zhu, W.T. Chen, V. Sanjeev, A. Zaidi, and F. Capasso, "Achromatic Metalens over 60 nm Bandwidth in the Visible." In *CLEO: QELS_Fundamental Science* (pp. FM1H-2) (2017).
57. S. Wang, C. Zhou, Z. Liu, and H. Li, "Design and analysis of broadband diffractive optical element for achromatic focusing." In *Holography, Diffractive Optics, and Applications VII* (Vol. 10022, p. 100221J) (2016).
58. V. N. Mahajan, G. M. Dai, "Orthonormal polynomials in wavefront analysis: analytical solution," *J. Opt. Soc. Am. A*, 24 (9), (2007).